Int. J. Electrochem. Sci., 15 **(2020)** 109 – 120, doi: 10.20964/2020.01.26

International Journal of ELECTROCHEMICAL SCIENCE
www.electrochemsci.org

Research on the Corrosion Behavior of 14Cr12Ni3Mo2VN Stainless Steel in Different Concentrations of NaCl Solution

Quande Li[1,2,3], Huimin Meng[1,],Randou[1],Xiufang Gong[2,3],Bin Long[2,3],Rong Ni[2,3], Xianlong Gong[2,3], Jun Dai[2,3]*

[1]Institute of Advance Materials and Technology, University of Science and Technology Beijing, Beijing 100083, China
[2] State Key Laboratory of Long-life High Temperature Materials,Deyang 618000, China;
[3] Dongfang TurbineCo.,LTD, Deyang 618000, China;
[*]E-mail: menghm16@126.com

Received: 9 September 2019 / *Accepted:* 29 October 2019 / *Published:* 30 November 2019

The corrosion behavior of 14Cr12Ni3Mo2VN martensitic stainless steel at different chloride ion concentrations was investigated by using the open circuit potential,electrochemical impedance spectroscopy,potentiodynamic polarization,Mott-Schottkycurves,scanning electron microscopy, energy dispersive spectroscopy and laser scanning confocal microscopy. It was found that with increasing concentrations of Cl^-, the open circuit potential constantly shifted in the negative direction, and the pitting potential, impedance value and protection potential of the passivation film all continuously decreased. Meanwhile, the main density N_d of a passivation film was obviously enhanced, and the number of point defects inside the passivation film and channels for corrosion medium transmission also increased.The corrosion resistance of thematerial continuously decreased with an increase in the concentration of Cl^-, leading to an increase in thecorrosion tendency of the steel. Fe and Cr in a corrosion pit selectively dissolved.Fe migrated out of the pit in the form of an ion, whereas Cr deposited in the form of an oxide in the corrosion pit. The corrosion pattern of the material surface changed from circular pitting to linear corrosion along the material surface with increasing chloride ion concentration, but the depth of the corrosion pit did not significantly increase.

Keywords: Stainless steel; Blade;Steam turbine; Electrochemistry; Corrosion

1. INTRODUCTION

Compared with 12Cr13, 14Cr12Ni3Mo2VN martensitic stainless steel shows better toughness,high-temperature thermal strength, performance stability, high-temperature oxidation resistance and steam corrosion resistance because of the addition of Mo, V, N and other alloy elements and is widely used in the manufacture of supercritical, final-stage turbine blades.A low-pressure final-stage blade of a steam turbine in a wet steam zone is not only subjected to high speed rotation and

static stress brought by airflow but is also exposed to oxygen corrosion, acid corrosion and other corrosive effects[1,2,3,4], which is completely different from its situation in a dry steam zone.

Finite element tools and fracture mechanics theory were used to study the life of steam turbine blades that had corrosion or defects, and to estimate the residual life of blades that had been operating for many years,but research on the specific conditions for turbine blades corrosion is not indicate[5,6,7,8,9].At present, research on the corrosion behavior of turbine blades at the last stage is mainly focused on determining corrosion factors (such as Cl^- in condensing water and dissolved oxygen) and the corrosion process through investigating corroded blades. However, research on the effect of Cl^- concentration in water condensation on the corrosion behavior of turbine blades is rarely reported[10,11]. Therefore, it is necessary for the safe operation of steam turbines to directly study the influence of Cl^- concentration on blade corrosion[12,13].Herein, the exact corrosion behavior and process of 14Cr12Ni3Mo2VN martensitic stainless steel was investigated, and the related corrosion mechanism was discussed.The experimental results can provide a theoretical basis and data support for practical steam turbine operation and choice of blade material.

2. EXPERIMENTAL

2.1 Working electrode preparation

14Cr12Ni3Mo2VN martensitic stainless steel specimens were used in this study, and their chemical composition is shown in Table 1.

Table 1. Chemical composition of 14Cr12Ni3Mo2VN martensitic stainless steel

Alloy	C	Si	Mn	S	P	Cr	Ni	Mo	V	N	Fe
wt%	0.15	0.12	0.75	0.073	0.013	11.50	2.97	1.61	0.28	0.034	balance

2.2 Experimental

The samples (10 mm×10 mm×10 mm) were cold-mounted with an epoxy resin to prevent crevice corrosion of the samples, and a 1 cm^2 exposed area was used as a working electrode. Before the experiment, the working electrode was polished step by step to a specular finish with a grinding machine, washed in distilled water and eventually dried by hot air just before being introduced into the electrochemical set-up.The tests were performed with a conventional three-electrode set-up. A platinum plate was used as a counter electrode, and an SCE (saturated calomel electrode) was used as a reference electrode.The experimental electrochemical media were NaCl solutions with different concentrations of 100, 200, 300 and 400 $mmol \cdot L^{-1}$.

Before the electrochemical testing, the working electrode was immersed in NaCl solution injected with 99.999% argon for 72h. Before measuring, the open circuit potential (OCP vs. SCE) was obtained after 30 min of running and stabilization. The potentiodynamic measurement rate was set to 1

$mV \cdot s^{-1}$, and the scanning range started from -500 mV(vs. SCE) and progressed to an anodic potential value. When the anodic polarization current density reached 1 $mA \cdot cm^{-2}$, reverse scanning was immediately carried out until intersecting with the anodic polarization curve, and then the test was stopped. Electrochemical impedance spectroscopy (EIS) measurements were carried out in a frequency range of 10^{5}-10^{-2} Hz with an amplitude of 10 mV. ZSimpWin software was used for data fitting analysis.A Mott-Schottky measurement was taken between -0.5 and 1.2 V (vs. SCE) with an ac signal amplitude of 10 mV. The test frequency was 1 kHz, and each parallel sample was tested at least 3 times for all of the above measurements.

After testing, the samples were rinsed with ethanol and deionized water and dried with cold air. The corrosion micromorphology of the working electrode surface was observed by a Zeiss EVO-18 scanning electron microscope, and the composition was measured by energy dispersive spectroscopy(EDS). The depth of the corrosion pit was measured by an OLYMPUS OLS5000 laser scanning confocal microscope.

3. RESULTS AND DISCUSSION

3.1 Open circuit potentials

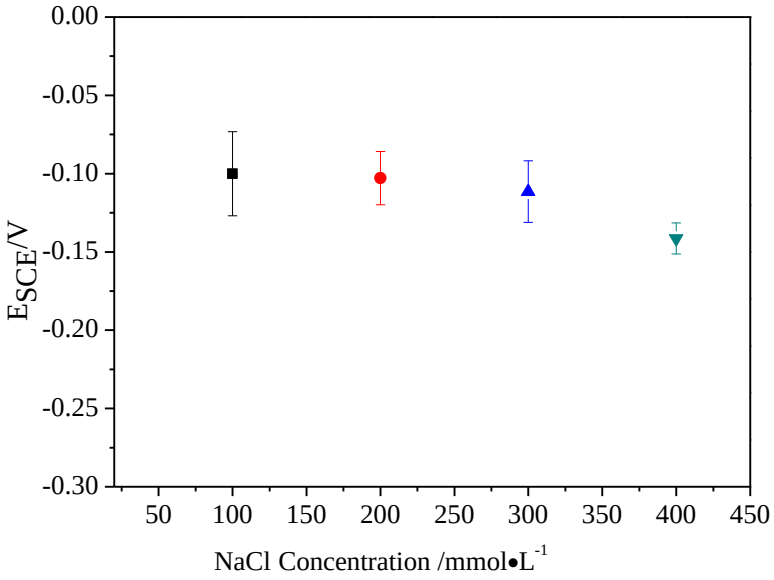

Figure 1. Open circuit potentials for 14Cr12Ni3Mo2VN martensitic stainless steel in deaeratedNaCl solutions with different concentrations.

The open circuit potentials of 14Cr12Ni3Mo2VN martensitic stainless steel in a NaCl solution of 100~400 $mmol \cdot L^{-1}$ are depicted in Fig. 1. The open circuit potential of 14Cr12Ni3Mo2VN stainless steel shifted negatively with increasing NaCl concentration, and the most negative potential of the sample was obtained by adding 400 $mmol \cdot L^{-1}$NaCl solution[14,15].

The more negative the open circuit potential is, the greater the corrosion tendency [16]. Thus, the electrochemical activity of 14Cr12Ni3Mo2VN stainless steel increases with increasing NaCl concentration[17].

3.2 Potentiodynamic polarization

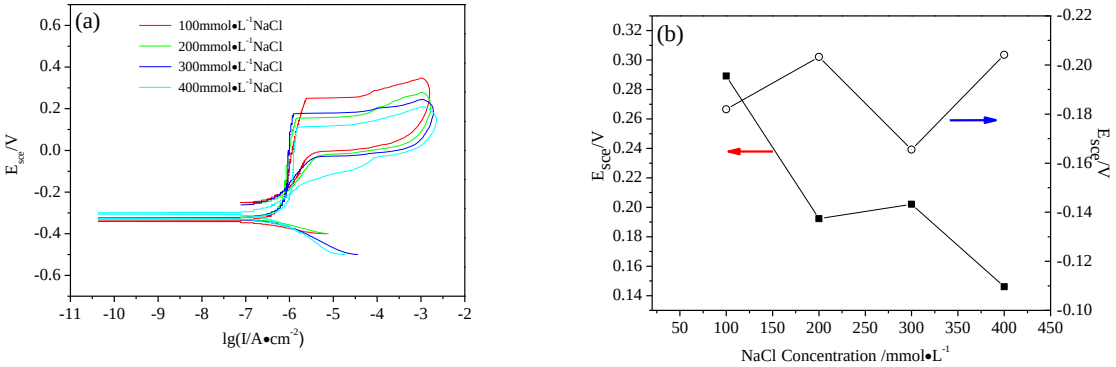

Figure 2. The potentiodynamic polarization curves of 14Cr12Ni3Mo2VN martensitic stainless steel samples in different concentrations of NaCl solution:(a)potentiodynamic polarization and (b)pitting potential and protection potential.

The potentiodynamic polarization curves of 14Cr12Ni3Mo2VN martensitic stainless steel samples in different concentrations of NaCl solution are shown in Fig. 2a.The potential value corresponding to the current density rapidly increasing to 100 μA·cm^{-2} on the polarization curve was the pitting potential. The potential at the intersection of the polarization curve and the anode polarization curve was the protection potential[18].All curves of the cathode polarization slope in Fig. 2a are very close, indicating that there is no obvious effect of the addition of NaCl on the cathode polarization rate of 14Cr12Ni3Mo2VN stainless steel.The addition of NaCl mainly affects the anode process[19].

With increasing NaCl concentration, the pitting and protection potentials of the 14Cr12Ni3Mo2VN sample showeddecreasing trends (Fig. 2b). The self-repairing ability of the passivation film became weakened, and the pitting sensitivity increased, which resulted in the corrosion resistance of the passivation film also decreasing [20,21].However, it is noted that the corrosion potential in Fig. 2a is more negative than the open circuit potential in Fig. 1, which is caused by the cathode polarization of the sample in the electrochemical polarization test.

A hysteresis ring and peak current density appear in the dynamic potential polarization curves during the backsweep at different concentrations. For the backsweep of potential, the current density does not immediately decrease, as there was a section where it increased before starting to decrease.This is because the passivated film on the surface of the 14Cr12Ni3Mo2VN stainless steel electrode was broken down during forward scanning, leading to pitting corrosion occurring on the surface of the electrode[22].A blocking area was formed due to the accumulation of corrosion products in the anode corrosion pit, resulting in an increase in the concentration of metal cations in the

occlusion area. To maintain electrical neutrality in the corrosion pit, Cl^- moves from the outside of the corrosion pit and continuously migrates and accumulates inside of the corrosion pit. As a result, the concentration of Cl^- in the hole constantly increases.Due to the high conductivity of concentrated salt solution in the corrosion area, the internal resistance of an occluded battery is very low, and corrosion is ongoing [23,24].At the same time, the solubility of oxygen is very low, and diffusion is difficult, leading to the development of pitting corrosion and hinderingthe repair of the metal passivation film.Even the backsweep in the negative potential direction could not immediately prevent the further expansion of pitting corrosion, resulting in a continuous increase of current density[25].However, each backsweep curve intersects the forward sweep curve at a certain potential, and then the current density remains lower than that of the forward sweep, indicating that a protective passivation film can be formed on the surface of each sample at this time.Unfortunately, with increasing concentrations of chloride ions, the protection potential gradually decreases, as shown in Fig. 2b, indicating the increasing difficulty of repairingthe corroded passivation film [26].

3.3 Electrochemical impedance spectroscopy

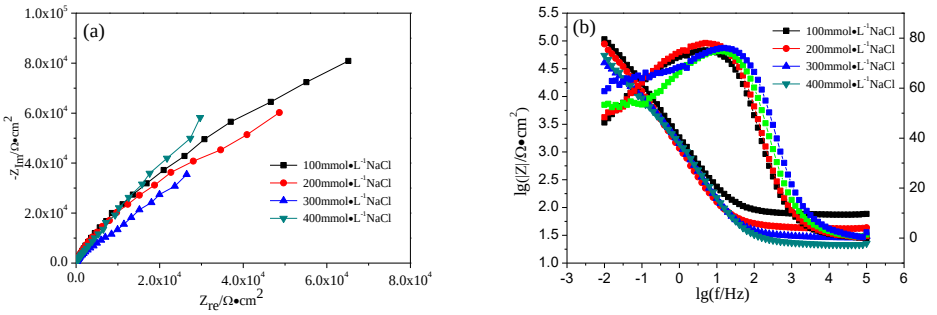

Figure 3. Electrochemical impedance spectroscopy of 14Cr12Ni3Mo2VN martensitic stainless steel samples in different concentrations of NaCl solution:(a)Nyquist and(b)Bode.

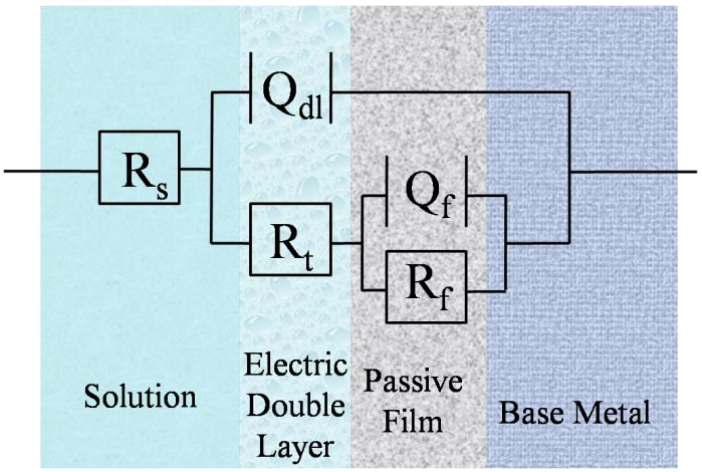

Figure 4. Equivalent circuit model for electrochemical impedance spectroscopy.

The electrochemical impedance spectroscopy test results of 14Cr12Ni3Mo2VN stainless steel in different NaCl concentrations can be seen in Fig. 3.The impedance of each system decreases with increasing NaCl concentration, which indicates that the protection of the passivation film on the surface of 14Cr12Ni3Mo2VN stainless steel becomes worse, the corrosion rate increases and the corrosion resistance decreases with increasing NaCl concentration[27].

The electrochemical impedance spectroscopy at different NaCl concentrations was analyzed by the equivalent circuit shown in Fig. 4 (see Table 2) [28],where R_s is the solution resistance, CPE(Q_f) is the passivation film capacitance, R_f is the passivation film resistance, CPE(Q_{dl}) and R_t are the capacitance and charge transfer resistance of the surface double layer, respectively, andCPE(Q) is generally used for the in-uniform distribution of the stainless steel surface current and high surface roughness.The CPE impedance value can be calculated by the following formula:

$$Z_Q = (j\omega)^{-n}/Y_0 \quad (1)$$

where Y_0 is the admittance modulus of CPE, omega is the angular frequency, and n is the diffusion exponent of the CPE. Its value range is set to $0 \le n \le 1$. When n=0.5, the CPE is considered a Warburg impedance.When n=1, the CPE is considered to be the ideal capacitance and when $0.5 < n < 1$, the CPE is in a middle state between the above-mentioned states.As shown inTable 2, in the 400 mmol·L^{-1}NaCl solution, the R_{fmin} of the 14Cr12Ni3Mo2VN martensitic stainlesssteel is 1.14×10^5 Ω·cm^2.With decreasing NaCl concentration, the R_f gradually increases, which indicates that the passivation film impedance increases,improving the protection[29,30]. The corrosion resistance of the material fitted by the equivalent circuit is in good agreement with the open circuit potential and potentiodynamic polarization test results.

Table 2. Parameters of the equivalent circuit

Concentrations of NaCl /mmol·L^{-1}	R_s/(Ω·cm^2)	Q_{dl}		R_t/(Ω·cm^2)	Q_f		R_f/(Ω·cm^2)
		Y_0/(Ω^{-1}·cm^{-2}·S^{n1})	n_1		Y_0/(Ω^{-1}·cm^{-2}·S^{n2})	n_2	
100	75.21	2.73×10^{-5}	0.90	1.46×10^4	1.61×10^{-5}	0.52	5.38×10^5
200	42.29	3.97×10^{-5}	0.92	2.67×10^4	2.84×10^{-5}	0.64	3.03×10^5
300	29.06	3.74×10^{-5}	0.92	1.18×10^4	4.59×10^{-5}	0.63	2.30×10^5
400	22.19	3.16×10^{-5}	0.93	3.56×10^4	3.92×10^{-5}	0.72	1.14×10^5

3.4 Mott-Schottky

When Cl^- exists in the solution, it will compete with OH^- in adsorbing on the surface of stainless steel. Further increasing the concentration of NaCl will result in more Cl^- adsorption on the electrode surface, thus accelerating the corrosion.The passivation film formed on the surface of a metal or alloy usually has semiconductor properties[31,32]. When the passivation film contacts the solution, a space charge layer will be formed on the side of the passivation film, and a Helmholtz layer will be formed on the side of the solution[33].At this time, the solution and the semiconductor film carry opposite charges, and the excess charge of the semiconductor film will be distributed in a space charge layer[34,35].When the space charge layer is in a depleted state, the capacitance of the space charge

layer and the measured electrode potential can be described and analyzed by the Mott-Schottky equation[36].

The space charge capacitance has the following relationship with the measured potential:

$$\frac{1}{C^2} = \frac{2}{\varepsilon\varepsilon_0 e N_d A^2}\left(E - E_{fb} - \frac{kT}{e}\right) \quad (2)$$

$$\frac{1}{C^2} = -\frac{2}{\varepsilon\varepsilon_0 e N_a A^2}\left(E - E_{fb} - \frac{kT}{e}\right) \quad (3)$$

$$W = \left[\frac{2\varepsilon\varepsilon_0}{eN_d}\left(E - E_{fb} - \frac{kT}{e}\right)\right]^{\frac{1}{2}} (4)$$

where C is the space charge layer capacitance of the passivation film, F; E is the scanning potential, V; E_{fb} is the flat band potential, V; ε_0 is the vacuum dielectric constant, 8.85×10^{-14} F·cm^{-1}; ε is the relative dielectric constant at 15.6; N_D and N_A represents the donor and acceptor densities for n-type and p-type semiconductors, respectively, cm^{-3}; A is sample area, which is set at1 in this paper, cm^2; K is the Boltzmann constant, 1.38×10^{-23}J·K^{-1}; e is the electron charge, 1.6×10^{-19}C; T shows the thermodynamic temperature, K; and W is the thickness of the passivation film, 10^{-10} m.

Equation (2) represents n-type semiconductor characteristics of the passivation film, while Equation (3) shows that of the p-type. Equation (4) represents its thickness.Fig. 5 shows the Mott-Schottky curve for stainless steel in different concentrations of chloride ion solutions. It can be seen that the Mott-Schottky curve has roughly the same variation trend with 2 intervals[37].The potential range of the first interval is -0.5-0.4 V. The slope of the fitted straight line is positive,representing an n-type semiconductor. The potential range of the second interval is 0.4~1.2 V, where the slope is negative, representinga p-type semiconductor.The main density of N_d is one of the important parameters for describing the passivation properties of stainless steel. Table 3 shows the N_d value calculated by fitting the -0.5-0.4 V region of the Mott-Schottky curve (Equation (2)).With increasing NaCl concentration, the main density N_d of the passivation film donor significantly increases[38]. The point defects in the passivation film increase, and the channels for corrosion medium transfer increase. Furthermore, the resistance of the charge transfer decreases, which makes the charge transfer and electrode reaction easier.According to Equation (4), when N_d increases, the thickness of the passivation film W decreases and the stability of the passivation film becomes worse, showing that its corrosion resistance decreases[39]. This indicates that with increasing NaCl concentration in solution, the point defects of the passivation film on the surface increase, forming more channels conducive to Cl^- transfer and promoting its adsorption on the surface of the stainless steel matrix, thusfurther increasing the active point on the surface to promote pitting[40].According to the above results, the increase of Cl^- concentration promotes the increase inthe point defect density of the stainless steel passivation film and reduces its thickness and stability, leading to an accelerating corrosion occurrence[41]. The above result is consistent with the electrochemical impedance spectroscopy.

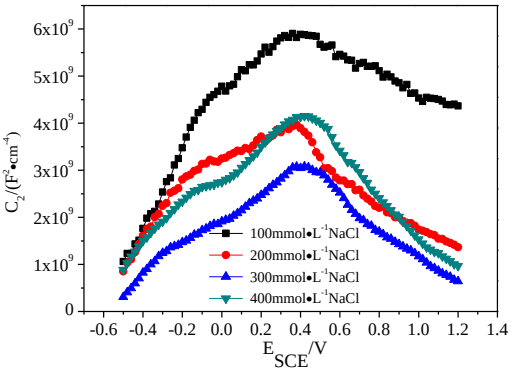

Figure 5. The Mott-Schottky curve of 14Cr12Ni3Mo2VN martensitic stainless steel samples in different concentrations of NaCl solution.

Table 3. Donor current density

Concentrations of NaCl /mmol·L^{-1}	$N_d/(10^{21}$ $cm^{-3})$
100	0.909
200	2.787
300	2.620
400	2.801

3.5 Morphology and composition analysis

The etched pit morphology results are shown in Fig. 6.In a solution with a low NaCl concentration, the pitting pattern of the 14Cr12Ni3Mo2VN stainless steel surface presents a relatively regular circular pitting pattern.As the concentration of NaCl increased, the morphology of the corrosion pit gradually became more complex. The pitting on the sample surface was measured by using a laser scanning confocal microscope (LSCM, Fig. 7). There was no significant increase in the depth direction of the observed corrosion pit, while more corrosion developed along the sample surface.Pyun and Park also found that with increasing NaCl concentration in a Cl^- containing solution, the pitting morphology of alloy 600 showed a trend of increasing roughness and more complex morphology [42].

Typical corrosion pits of each surface sample were selected and marked as three different areas (A), (B) and (C)(see Fig. 6). An energy dispersive spectroscopy (EDS) analysis was conducted on the selected areas. The atomic ratio between Cr and Fe along with the oxygen content of the three areas are shown in Table 4.

According to the EDS analysis results, the corrosion products are mainly composed of Fe and Cr. Corrosion products in the pits are mainly composed of Cr[43]. The content of Cr corrosion products inside the pits is higher than that on the outside, but the content trend of Fe is totally opposite that of Cr. The above observationindicates that when pitting corrosion occurs on the surface and

spreads inward, the Fe and Cr undergo selective dissolution. Fe quickly migrates out from the corrosion pit[44,45], while Cr slowly migrates and deposits to a certain extent, resulting in a high Cr content in the pit interior and aggregated Fe outside of the pit area[46].In addition, the O content of the sample in the corrosion pit is much higher than that in other areas, indicating that Cr oxides exist in the corrosion products. That is, during the corrosion of stainless steel, Fe is dissolved into the medium in the form of ions, while Cr is deposited in the form of oxides[47,48].

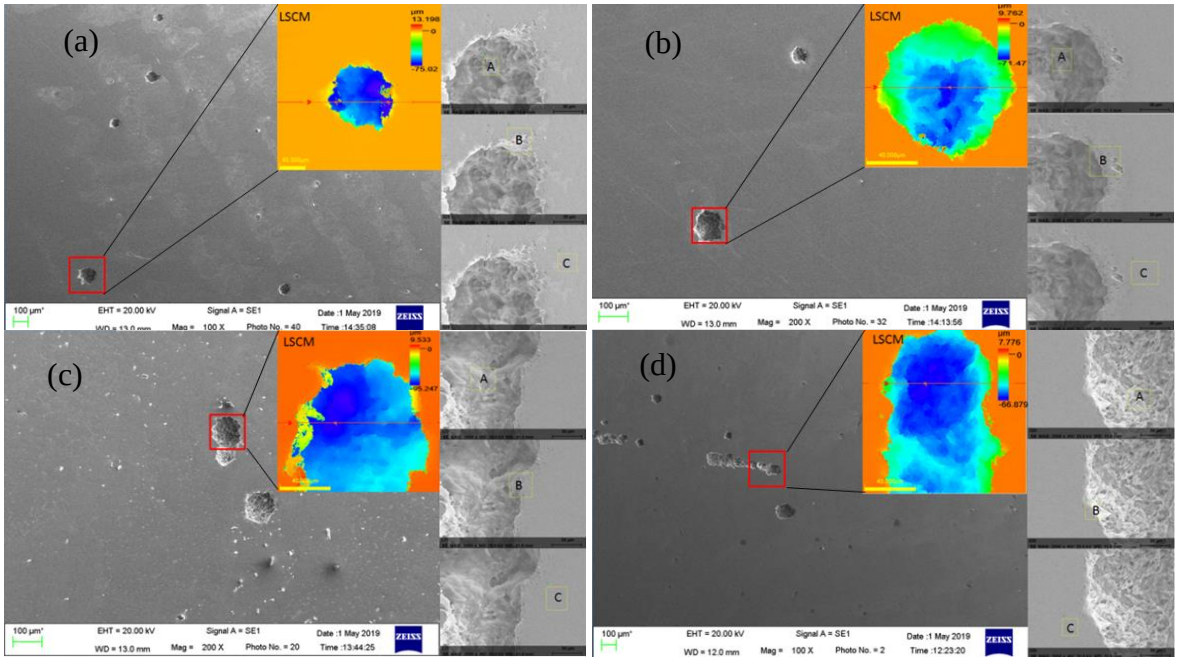

Figure 6. The pit morphology of 14Cr12Ni3Mo2VN martensitic stainless steel samples in different concentrations of NaCl solution:(a)100 mmol·L^{-1},(b)200 mmol·L^{-1},(c)300 mmol·L^{-1}, and (d)400 mmol·L^{-1}.

Table 4. EDS analysis of the selected region in Fig.5

Concentrations/ mmol·L^{-1}	100			200			300			400		
Region	A	B	C	A	B	C	A	B	C	A	B	C
Cr/Fe(atom/atom)	1.12	0.16	0.13	1.05	0.2	0.25	0.21	0.19	0.13	0.28	0.18	0.14
O(wt%)	2.76	1.21	0.35	19.19	4.23	1.16	3.41	7.68	0.93	9.41	7.67	7.90

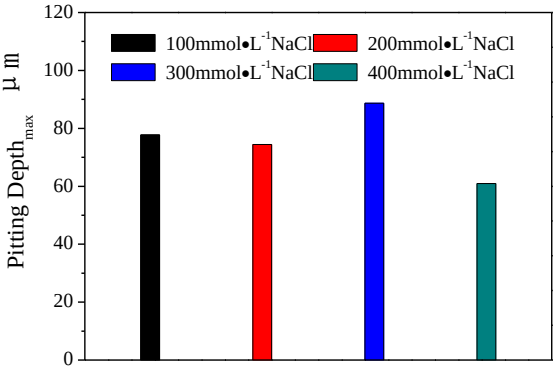

Figure 7. Maximum depth of corrosion pits in14Cr12Ni3Mo2VN martensitic stainless steel samples in different concentrations of NaCl solution.

4. CONCLUSIONS

With increasing concentrations of Cl^-, the open circuit potential of 14Cr12Ni3Mo2VN martensitic stainless steel constantly shifted in the negative direction, and the pitting potential, impedance value and protection potential of the passivation film all continuously decreased. Meanwhile, the main density N_d of the passivation film obviously enhanced, and point defects inside the passivation film and channels of corrosion medium transmission also increased. The corrosion resistance of the material continuously decreased with an increase in the Cl^- concentration, leading to a rising corrosion tendency of the steel.

When pitting corrosion occurs on the surface and begins spreadinginto the pits, Fe and Cr undergo selective dissolution.Fe will migrate out in the form of an ion, and Cr will deposit in the form of an oxide in the corrosion pit.The corrosion pattern of the material surface changed from circular pitting to linear corrosion along the material surface with increasing chloride ion concentration, but the depth of the corrosion pit did not significantly increase.

ACKNOWLEDGEMENTS
This work was supported by the fund of the State Key Laboratory of Long-life High Temperature Materials(No. DTCC28EE190230)

References

1. Masoud Vatanmakan, Esmail Lakzian, Mohammad Reza Mahpeykar, *Energy,* 147 (2018) 70.
2. Bernd M. Schönbauer, Stefanie E. Stanzl-Tschegg, Andrea Perlega, Ronald N. Salzman,Neville F. Rieger, Alan Turnbull, Shengqi Zhou, Mikolaj Lukaszewicz, David Gandy, *Eng. Fract. Mech.*,147 (2015) 158.
3. D. Ziegler, M. Puccinelli, B. Bergallo, A. Picasso, *Cas. Stud. Eng. Fail. Anal.*,1 (2013) 192.

4. D.G. Hattingh, M.N. James, M. Newby, R. Scheepers, P. Doubell, *Theor. Appl. Fract. Mec.*, 83 (2016) 125.
5. C. Booysen, P.S. Heyns, M.P. Hindley, R. Scheepers, *Int. J. Fatigue*, 73 (2015) 17.
6. Marko Katinić, Dražan Kozak, Ivan Gelo, Darko Damjanović, *Eng. Fail. Anal.*, 106 (2019) 104136.
7. Junzhou Huo, Debin Sun, Hanyang Wu, Weizheng Wang, lin Xue, *Eng. Fail. Anal.*, 106 (2019) 104159.
8. Zixu Guo, Dawei Huang, Xiaojun Yan, Xiaoyong Zhang, Mingjing Qi, *Jun Fan, Int. J.Fatigue*, 131 (2020) 105298.
9. S. Cano, J.A. Rodriguez, J.M. Rodriguez, J.C. Garcia, F.Z. Sierra, S.R. Casolco,M. Herreraa, *Eng. Fail. Anal.*, 97 (2019) 579.
10. Goutam Das, Sandip Ghosh Chowdhury, Ashok Kumar Ray,Swapan Kumar Das, Deepak Kumar Bhattacharya, *Eng. Fail. Anal.*, 10 (2003) 85.
11. A.P. Tschiptschin, C.R.F. Azevedo, *Eng. Fail. Anal.*, 12 (2005) 49.
12. Yu-jiang Xie, Mao-cai Wang, Ge Zhang, Min Chang, *Eng. Fail. Anal.*, 13 (2006) 1429.
13. Hyojin Kim, *Eng. Fail. Anal.*, 18 (2011) 907.
14. M. Stefanoni, U.Angst, B.Elsener, *Corros. Sci.*, 98 (2015) 610.
15. Farzin Arjmand, Lefu Zhang, Jiamei Wang, *Nuclear Engineering and Design*, 322 (2017) 215.
16. Karthikeyan Selvam, Jaskaran Saini, Gopinath Perumal, Aditya Ayyagari, Riyadh Salloom,Riya Mondal, Sundeep Mukherjee, Harpreet Singh Grewal, Harpreet Singh Arora, *Tribol. Int.*, 134 (2019) 77.
17. C.J. Scheuer, F.A.A. Possoli, P.C. Borges, R.P. Cardoso, S.F. Brunatto, *Electrochim. Acta*, 317 (2019) 70.
18. Heon-Young Ha, Tae-Ho Lee, Chang-Geun Lee, Hanme Yoon, *Corros. Sci.*, 149 (2019) 226.
19. Xudong Chen, Yusheng Li, Yuntian Zhu, Yakui Bai, Bin Yang, *Appl. Surf. Sci.,* 481 (2019) 1305.
20. N. Ebrahimi, M. Momeni, A. Kosari, M. Zakeri, M.H. Moayed, *Corros. Sci.*, 59 (2012) 96.
21. Jian Wang, Yishi Cui, Jingang Bai, Nan Dong, Ying Liu, Caili Zhang, Peide Han, *Mater. Lett.* ,252 (2019) 60.
22. I.G. Ogunsanya, C.M. Hansson, *Materialia*, 6 (2019) 100321.
23. G. Tranchida, M. Clesi, F. Di Franco, F. Di Quarto, M. Santamaria, *Electrochim. Acta.*, 273 (2018) 412.
24. J. Li, C.W. Du, Z.Y. Liu, X.G. Li, M. Liu, *Constr. Build. Mater.*, 189 (2018) 1286.
25. Xuanpeng Li, Yang Zhao, Wenlong Qi, Junfeng Xie, Jidong Wang, Bin Liu,Guanxin Zeng, Tao Zhang, Fuhui Wang, *Appl. Surf. Sci.,* 469 (2019) 146.
26. M.J.K. Lodhi, K.M. Deen, M.C. Greenlee-Wacker, Waseem Haider, *Addit. Manuf.*, 27 (2019) 8.
27. Fenfen Yang, Huijun Kang, Enyu Guo, Rengeng Li, Zongning Chen, Yanhua Zeng,Tongmin Wang, *Corros. Sci.*, 139 (2018) 333.
28. Hong Luo, Qiang Yu, Chaofang Dong, Gang Sha, Zhenbao Liu, Jianxiong Liang,Li Wang, Gang Han, Xiaogang Li, *Corros. Sci.*, 139 (2018) 185.
29. Odhiambo John Gerald, Li WenGe, Li Zhang, Zhao YuanTao, Li Cheng Lon, *Mater. Chem. and Phys.*, 239 (2020) 122010.
30. L. Pan, C.T. Kwok, K.H. Lo, *J. Mater. Process. Tech.*, 277 (2020) 116448.
31. J. Izquierdo, L. Martín-Ruíz, B.M. Fernández-Pérez, R. Rodríguez-Raposo, J.J. Santana,R.M. Souto, *Electroanal. Chem.*, 728 (2014) 148.
32. Zhenwei Yan, Xianjie Yuan, Zhaojun Tan, Mingqi Tang, Zaiqiang Feng, *Int. J. Electrochem. Sc.*,13(2018)353.
33. Ibrahim M. Gadala, Akram Alfantazi, *Appl. Surf. Sci.,* 357 (2015) 356.
34. Lv Jinlong, Huijin Jin, Liang Tongxiang, *Mater. Lett.*, 256 (2019)126640.
35. Tigang Duan, Wenshan Peng, Kangkang Ding, Weimin Guo, Jian Hou, Wenhua Cheng, Shaotong Liu, Likun Xu, *Ocean. Eng.*, 189 (2019) 106.
36. A. Fattah-alhosseini, S. Vafaeian, *J. Alloy. Compd.*, 639 (2015) 301.

37. Alberto Adan Mas, Teresa M. Silva, Liliane Guerlou-Demourgues, Maria Fatima Montemor, *Electrochim. Acta.*, 289 (2018) 47.
38. Sabrina Marcelin, Benoit Ter-Ovanessian, Bernard Normand, *Electrochem. Commun.*, 66 (2016) 62.
39. M. BenSalah, R. Sabot, E. Triki, L. Dhouibi, Ph. Refait, M. Jeannin, *Corros. Sci.*,86 (2014) 61.
40. L.V. Taveira, M.F. Montemor, M. Da Cunha Belo, M.G. Ferreira, L.F.P. Dick, *Corros. Sci.*,52 (2010) 2813.
41. Yazhou Zhao, Tao Pan, Xiaotong Yu, Da Chen, *Corros. Sci.*, 158 (2019) 108097.
42. Jin-Ju Park, Su-Il Pyun, *Corros. Sci.*, 46 (2004) 285.
43. Miranda, Jesualdo Pereira Farias, Luciano Andrei Bergmann, Jorge F. dos Santos, *J. Mater. Res. Technol.*, 2019;8(2):1878.
44. Y.Y. Li, Z.Z. Wang, X.P. Guo, G.A. Zhang, *Corros. Sci.*,147 (2019) 260.
45. Xiangfeng Zhang, Jun Wang, Hongyuan Fan, Dong Pan, *Appl. Surf. Sci.,* 440 (2018) 755.
46. Decheng Kong, Chaofang Dong, Xiaoqing Ni, Liang Zhang, Jizheng Yao,Cheng Man, Xuequn Cheng, Kui Xiao, Xiaogang Li, *J. Mater. Sci. Technol.*, 35 (2019) 1499. .
47. Sicong Shen, Xiaolong Song, Qizhen Li, Xinfeng Li, Ruihua Zhu, Gongxian Yang, *Mat. Sci. Eng.A.*, 740-741 (2019) 243.
48. Mirosław Szala, Karolina Beer-Lech, MariuszWalczak , *Eng. Fail. Anal.*, 77 (2017) 31.